Available online at www.sciencedirect.com
SCIENCE DIRECT®
Journal of Solid State Chemistry 177 (2004) 4149–4162
JOURNAL OF SOLID STATE CHEMISTRY
www.elsevier.com/locate/jssc

$Bi_{\sim 3.785}Cd_{\sim 3.575}Cu_{\sim 1.5}(PO_4)_{3.5}O_{5.5}$, a new arrangement of double ($n = 2$) and triple ($n = 3$) $[M_4Bi_{2n-2}O_{2n}]^{x+}$ polycationic ribbons in the bismuth-transition metal oxy-phosphate series

Marie Colmont, Marielle Huvé, Francis Abraham, Olivier Mentré*

Laboratoire de Cristallochimie et Physicochimie du Solide, CNRS UMR 8012, ENSCL, Université des Sciences et Technologies de Lille, BP.108, F-59652 Villeneuve d'Ascq Cedex, France

Received 9 March 2004; received in revised form 10 June 2004; accepted 28 June 2004

Abstract

This work is dedicated to investigation of new disordered bismuth-containing oxy-phosphates compounds with an original structure type. As previously observed in this series, they are formed of $[M_4Bi_{2n-2}O_{2n}]^{x+}$ polycationic ribbons of width n $O(Bi,M)_4$ tetrahedra, surrounded by PO_4 groups. In the new crystal structure type, double ($=D$), triple ($=T$) and tunnels ($=t$) alternate along a common axis obeying the $TtDtTtDt/TTtTTt$ sequence in respect to a nomenclature previously described and recalled in this work. The existence this new polymorph has first been detected by electron diffraction in a multi-phased sample. Then, the crystal structure type, i.e., the $TtDtTtDt/TTtTTt$ sequence, has been deduced from HREM images help to a contrast-interpreting code available for these series of polycations-formed compounds. The subsequent compounds formulation leads to a number of new materials that verify the general formula: $[Bi_2(Bi,M)_4O_4]_2$ $[Bi_4(Bi,M)_4O_6]_6$ $(PO_4)_{28}$ M_x, with $x \leqslant 12$ and $M = Cu^{2+}$, Cd^{2+} cations. Single crystals of the nominal $[O6Bi_{4.57}Cd_{3.43}]_4^{+8.57}$ $[O_6Bi_4Cd_4]_2^{+8}$ $[O_4Bi_2Cd_{3.56}Cu_{0.44}]_2^{+6}$ $(PO_4)_{28}$ $Cu_{10.86}$ have been prepared in a further stage and confirms the predicted crystal structure, $Bi_{\sim 3.785}Cd_{\sim 3.575}Cu_{\sim 1.5}(PO_4)_{3.5}O_{5.5}$, $a = 11.506(8)$ Å, $b = 5.416(4)$ Å, $c = 53.94$ (4) Å, $\beta = 90.10(1)^\circ$, $R_F = 0.0835$, $R_{wF} = 0.0993$, $SG = A2/m$, $Z = 8$. As already observed for other elements of this family such as $Bi_{\sim 1.2}M_{\sim 1.2}O_{1.5}(PO_4)$, $Bi_{\sim 6.2}Cu_{\sim 6.2}O_8(PO_4)_5$ or $Bi_{\sim 3}Cd_{\sim 3.72}M_{\sim 1.28}O_5(PO_4)_3$ (M = Cu, Co, Zn), this compound shows an additional example of PO_4 disorder due to the presence of mixed Bi^{3+}/M^{2+} sites at the edges of ribbons. The origin and consequence of this so-called disorder mostly occurring on PO_4 configurations is intensively discussed and has been characterized by infrared spectroscopy and by neutron diffraction on similar compounds. It is noticeable that the great number of antagonist PO_4 configurations may order along the b-axis within a large periodicity which involves incommensurate lattice.

Keywords: Bismuth oxide phosphate; Polycations; Crystal structure; X-ray diffraction; ED/HREM

1. Introduction

The study of several ternary systems as P_2O_5–Bi_2O_3–MO has allowed to point out and characterize new oxide-phosphates, e.g., $BiMPO_5$ (M = Co, Ni, Mn) [1–4], BiM_2PO_6 (M = Mg, Ca, Cu, Cd, Pb, Zn…) [5–12], $Bi_6A_x(PO_4)_4O_4$ (A = Bi, Sr, Pb, Cd, Ca, Li, Na, K) [13,14], $Bi_2MnPbO_4(PO_4)_2$ [15], $BiMn_6PO_{12}$ [16], $Bi_{\sim 1.2}M_{\sim 1.2}PO_{5.5}$ (M = Mn, Zn, Co) [17], $Bi_{\sim 6.2}Cu_{\sim 6.2}P_5O_{28}$ [18] and recently $Bi_{\sim 3}Cd_{\sim 3.72}M_{\sim 1.28}P_3O_{17}$ (M = Cu, Co, Zn) [19]. These compounds can be described by the association of isolated PO_4 tetrahedra sharing corners with MO_x polyhedra. Using this model, Bi^{3+} plays an interstitial role within the created frameworks. Nevertheless, this classical description does not allow to established topological relationships between the several structures and is not well suited to describe recently evidenced disordered materials [17–19].

By analogy with the fluorite type of δ-Bi_2O_3 formed of $OBi_4/\square Bi_4$ clusters ($\square$ stands for an oxygen vacancy), we established an original description [17] based on

*Corresponding author. Fax: +33-320-436-814.
E-mail address: mentre@ense-lile.fr (O. Mentré).

0022-4596/$ - see front matter © 2004 Elsevier Inc. All rights reserved.
doi:10.1016/j.jssc.2004.06.057

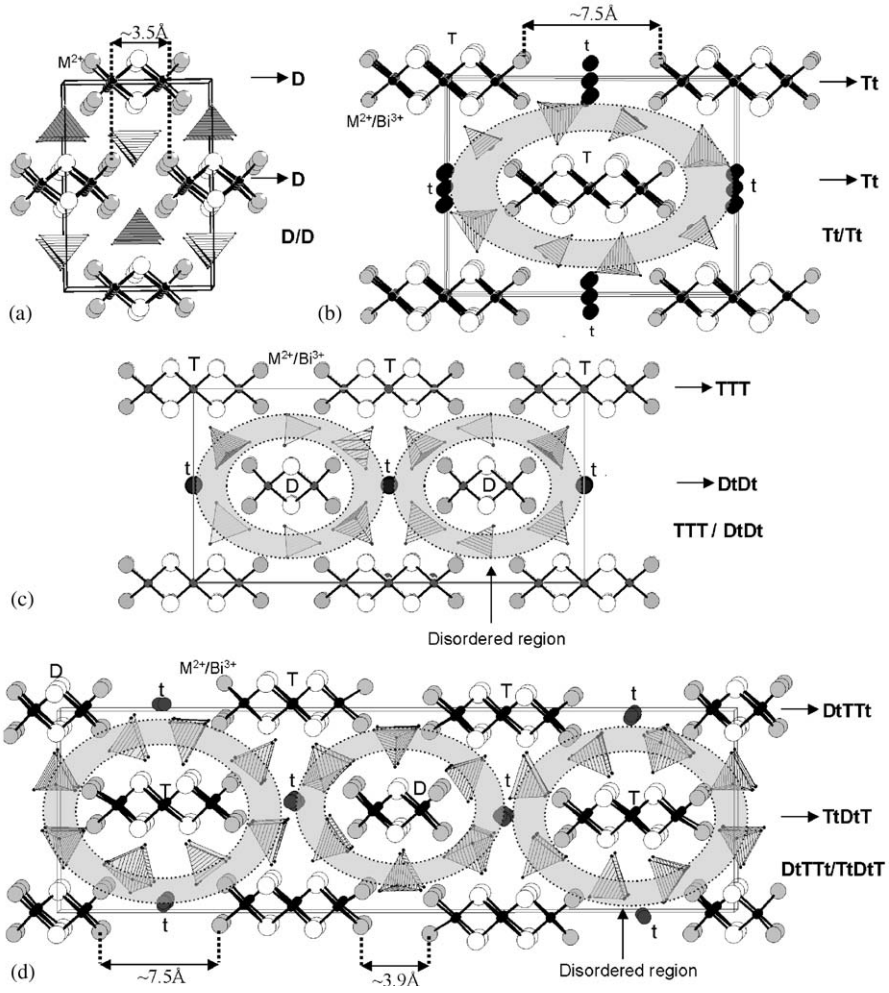

Fig. 1. Projection along b of the structures of oxide-phosphate compounds, showing the T, D, t nomenclature: (a) BiM_2PO_6, (b) $Bi_{\sim 1.2}M_{\sim 1.2}(PO_4)O_{1.5}$, (c) $Bi_3Cd_{3.72}Co_{1.28}O_5(PO_4)_3$ and (d) $Bi_{\sim 6.2}Cu_{\sim 6.2}(PO_4)_5O_8$. The gray crown pictures the disordered space existing in most of the structures because of the mixed nature of sites of ribbons edges (gray atoms).

phosphate groups and infinite bi-dimensional ribbon-like polycations growing along **b** (~5.2 Å) axis and parallel to (100) ($a \sim 11.5$ Å), two parameters common to all the previously cited materials. The polycations are built from edge-shared $O(Bi,M)_4$ tetrahedra of $n = 1, 2, 3\ldots$ tetrahedra width, the c parameter depending on the ribbons width and arrangement of ribbons. The eventual presence of mixed Bi^{3+}/M^{2+} sites, at the end of the ribbons, is responsible for a strong PO_4 disorder in the inter-ribbon space. In some cases, transition metals bonded by PO_4 corners occupy tunnels ($=t$) located between two subsequent ribbons. Within this description, a topological relation between the different materials was pointed out in term of double ($=D$) and triple ($=T$) ribbons arrangement. That led us to set a new nomenclature first announced in [19]. The code consists in using the appropriate T–D–t sequence along the c-axis centered at $x = 0$ and $x = \frac{1}{2}$ separated by/. Thus, BiM_2PO_6 ($c \sim 8$ Å) and $Bi_{\sim 1.2}M_{\sim 1.2}O_{1.5}(PO_4)_1$ ($c \sim 15$ Å) adopt a D/D and a Tt/Tt sequence, respectively. Both T and D cohabit in $Bi_{\sim 6.2}Cu_{\sim 6.2}O_8(PO_4)_5$ ($c \sim 38$ Å–$DtTTt/TtDtT$ sequence) and $Bi_{\sim 3}Cd_{\sim 3.72}M_{\sim 1.28}O_5(PO_4)_3$ ($c \sim 23$ Å–$TT/DtDt$ sequence) as shown in Fig. 1.

In this paper, we report the preparation, the electron diffraction and HREM study interpreted using a recently established code [20] and the average crystal structure of the new $Bi_{\sim 3.785}Cd_{\sim 3.575}Cu_{\sim 1.5}(PO_4)_{3.5}O_{5.5}$ oxy-phosphate showing the $TtDtTtDt/TTtTTt$ structure type with $a = 11.506(8)$Å, $b = 5.416(4)$Å, $c = 53.94(4)$Å, $\beta = 90.10(1)^\circ$ and $SG = A2/m$.

2. Experimental section

The different oxides reported in this paper have been prepared from stoechiometric mixtures of Bi_2O_3, CdO, MO (M = Cu, Co, Ni, Zn) and $(NH_4)_2HPO_4$. To avoid

the problem of volatile species removal during solid state preparative methods, which imply a several heating-regrinding steps reaction from 200 to 850 °C, the reactants have been dissolved in nitric acid and homogenized by magnetic stirring. A small amount of citric acid was added in order to complex and disperse the cations in the solution. It was heated at 150 °C up to total evaporation. Afterwards the resulting powder was dried, transferred in an alumina crucible and heated at 5 °C/h to 850 °C for 24 h and finally quenched to room temperature. The purity of the samples was checked by powder X-ray diffraction using a Siemens D-5000 diffractometer back monochromatized and Cu$K\alpha$ radiation.

Electron diffraction (ED) patterns and high-resolution images were obtained on a Jeol 200CX and a Jeol 4000EX (point resolution of 1.7 Å). In each case, the material was crushed and dispersed on a holey carbon film deposited on a Cu grid. The simulated HREM images have been calculated using the multi-slice method and the JEMS program [21].

The magnetic susceptibilities have been measured by the DC-extraction method using an Oxford-MAGLAB EXA 9 T apparatus. The applied field is 1 kOe upon heating from 5 to 300 K.

Single crystal X-ray diffraction data have been collected on a Bruker SMART CCD 1 K diffractometer (50 kV × 40 mA, Mo$K\alpha$) under the following conditions: a full reciprocal sphere corresponding to a total of 3×600 frames was collected (ω-scan, 40 s per frame) with a crystal-detector distance of 80 mm (due to the large c parameter). The intensities were extracted using the program SaintPlus 6.02 [22]. An absorption correction based on the crystal morphology was applied using the program XPREP of the SHELXTL block [23]. Data were re-corrected from the glass fiber and the area detector absorption using empirical corrections using the program SADABS [24] with a null μr value. The pertinent data of the reflections collection, treatment and refinement are summarized in Table 1.

Table 1
Crystal data, measurement, and structure refinement parameters for $Bi_{\sim 3.785}Cd_{\sim 3.575}Cu_{\sim 1.5}(PO_4)_{3.5}O_{5.5}$

Crystal data	
Crystal symmetry	Monoclinic
Space group	$A2/m$
Cell dimension (Å)	$a = 11.506(8)$ Å
	$b = 5.416(4)$ Å
	$c = 53.94(4)$ Å
	$\beta = 90.10(1)°$
	$a = 11.506(8)$ Å
Volume (Å^3)	$V = 3361.9(6)$ (Å^3)
Z	4
Data collection	
Equipment	Bruker SMART CCD
λ (Mo$K\alpha$ (graphite monochromator)) (Å)	0.71073
Density calc.	7.3085 g/cm^3
Color	Green
Scan mode	ω
Θ max (deg)	29.80
Recording reciprocal space	$-16 \leqslant h \leqslant 15$, $-7 \leqslant k \leqslant 7$, $-73 \leqslant l \leqslant 71$
Number of measured reflections	4840
Number of independent reflections	2361
μ (mm^{-1}) (for $\lambda K\alpha = 0.7107$ Å)	65.286
Limiting faces and distances (mm) from an arbitary origin	0.00 1.00 0.00 0.2100
	0.00 $\bar{1}$.00 0.00 0.2100
	$\bar{1}$.00 0.00 0.00 0.0214
	1.00 0.00 0.00 0.0166
	0.00 0.00 $\bar{1}$.00 0.0174
	0.00 0.00 1.00 0.0174
	1.00 0.00 5.00 0.0180
	1.00 0.00 $\bar{5}$.00 0.0127
Refinement	
Number of refined parameters	266
Refinement method	Least square on F
$R1(F)[I > 2\sigma I]/R1(F)$[all data]	0.0835/0.1008
$wR2(F^2)[I > 2\sigma I]/wR2(F^2)$ [all data]	0.0993/0.1087
$w = 1/(\sigma^2(F_0^2) + (0.0700*P)^2 +$ 0.00*P) with $P = (\mathrm{Max}(F_0^2, 0) + 2*F_c^2)/3$	
Goof	3.62
Max/min $\Delta\rho$ (e Å^{-3})	1.03/0.01e Å^{-3}

3. TEM study

For this series of compounds, an interpretation image code explaining HREM contrast, has been established. Using structural basic considerations, it allows the formulation necessary for the synthesis of new oxides [20]. One interesting advantage of the TEM is the exploration of powder crystal per crystal, considerably useful in a multiphase sample. In the treated case, first clues of a new polymorph have been observed on a minor phase among a mixture.

The powder sample prepared at 800°C for the nominal composition $BiCuCdPO_6$ mainly shows a compound with an A-centered orthorhombic cell with parameters $a \sim 11.5$ Å, $b \sim 5.3$ Å and $c \sim 38$ Å, that corresponds to the *TtDtTtDt/TTtTTt* crystal, e.g., $Bi_{\sim 6.2}Cu_{\sim 6.2}O_8(PO_4)_5$ type [18]. However the electron diffraction pointed out the presence of an additional phase. The a and b parameters obtained by the reciprocal space reconstitution are about 11.5 and 5.3 Å, respectively, which are parameters common to all the previous cited materials. The c parameter, closed to 54 Å, suggested the discovery of a new ribbons arrangement. Basic electron diffraction patterns (EDP) (Fig. 2) display modulation spots which have been

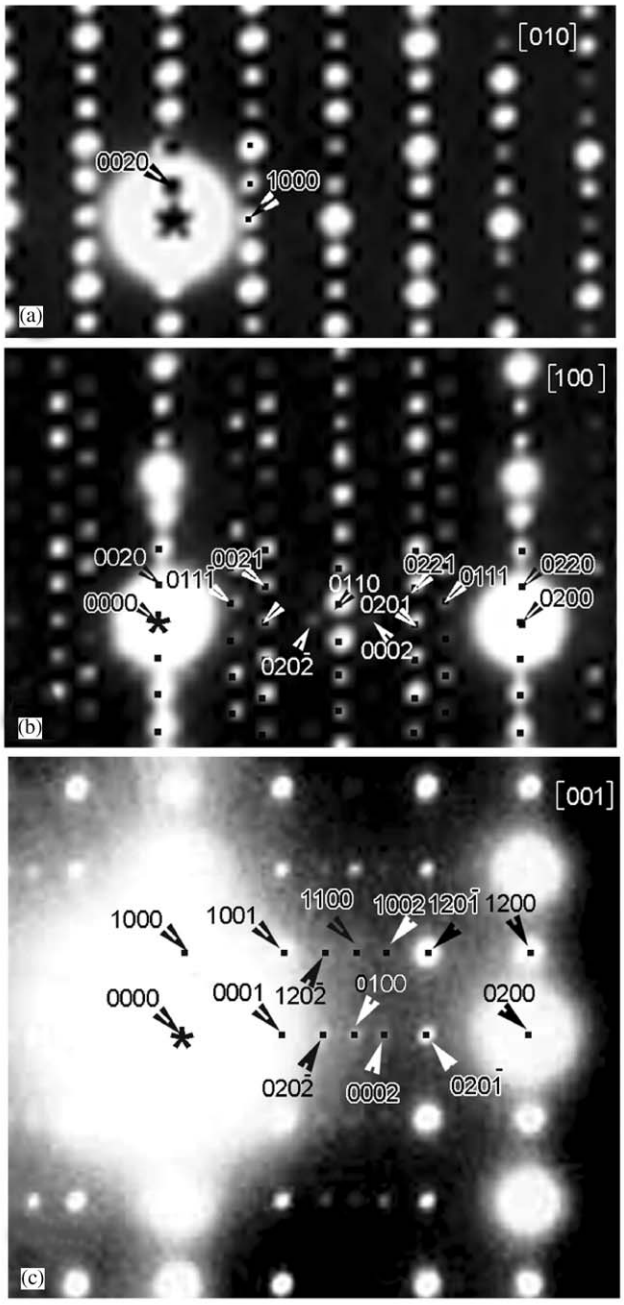

Fig. 2. Basic EDP: (a) [010], (b) [100] and (c) [001]. The modulation's spots are indexed with a modulation vector: $q^* = (2/3 - \varepsilon)B^*$.

indexed with a modulation vector $\mathbf{q}^* = (2/3 - \varepsilon)\mathbf{b}^*$. In order to assign the corresponding *D–T–t* sequence and finally to formulate the compound using the method described in [20], an HREM study has been performed. The [010] HREM image obtained in the same defocus/thickness conditions used to establish the interpretation image code is shown in Fig. 3. This image perpendicular to the infinite ribbons axis (*b*-axis) contains the information necessary to determine the size and ribbons organization.

3.1. Polycations sequence deduction

The analysis of the experimental image (Fig. 3a$_3$) is based on the code already established and available for *T–D–t* containing compounds:

- Double ribbons are localized in dark region between two white circles along (a) (Fig. 3a$_1$)
- Triple ribbons take place in dark region between two white crosses along (a) (Fig. 3a$_2$),
- Considering the wideness of "*D*" (~5 Å) and "*T*" (~8 Å), "*t*" tunnels are located between two ribbons separated by ~7 Å, as previously observed for other compounds [17–19]. It leads to the new *TtDtTtDt*/*TTtTTt* sequence (Fig. 3b).

3.2. Compound(s) formulation

As intensively discussed in [19] the *n*-tetrahedra wide polycations can be formulated $[E_4Bi_{2n-2}O_{2n}]^{x+}$ where *E* stand for the edges of ribbons positions (with possible mixed Bi^{3+}/M^{2+} nature) and Bi for the core of ribbons (solely Bi^{3+}). Furthermore, by analogy between the compounds already discovered so far empirical "formulation rules" have been proposed [18,19,24]:

- $D = [Bi_2(Bi,M)_4O_4]$ are surrounded by 6 PO_4 groups in the (*a*,*b*) plane.
- $T = [Bi_4(Bi,M)_4O_6]$ are surrounded by 8 PO_4 groups.
- The main formula is then, $[Bi_2(Bi,M)_4O_4]_2$ $[Bi_4(Bi,M)_4O_6]_6$ $(PO_4)_{28}$ t_6, where *t* corresponds to tunnels occupied by M^{2+} cations (Cd^{2+} or Cu^{2+}). The tunnels occupancy is variable and plays a charge balance role towards edges of ribbons Bi^{3+}/M^{2+} occupancies. At least can we empirically announce that along one b period, one tunnel could contain a maximum of 2 M^{2+} cations (involving *M–M* separations of $b/2 \sim 2.7$ Å). Then the structural formula is $[Bi_2(Bi,M)_4O_4]_2$ $[Bi_4(Bi,M)_4O_6]_6$ $(PO_4)_{28}$ M_x, with $x \leqslant 12$ and $M = Cu^{2+}$, Cd^{2+} cations (Fig. 3c)

4. Powder and single crystal syntheses

A great number of possible compositions which involves different edges of ribbons, Bi^{3+}/M^{2+} ratio and variable $M^{2+} = Cu^{2+}/Cd^{2+}$ ratio, and variable tunnel occupancies have been prepared in the Bi_2O_3–P_2O_5–CuO–CdO quaternary diagram. In most of the cases, the XRD powder patterns show evidence of the mixture of several structural types. Therefore few samples show either a single phase fully indexed using a slight monoclinic distortion that perturbs the orthorhombic $a \sim 11.5$ Å, $b \sim 5.5$ Å, and $c \sim 54$ Å unit cell. The reason for such symmetry lowering is developed in

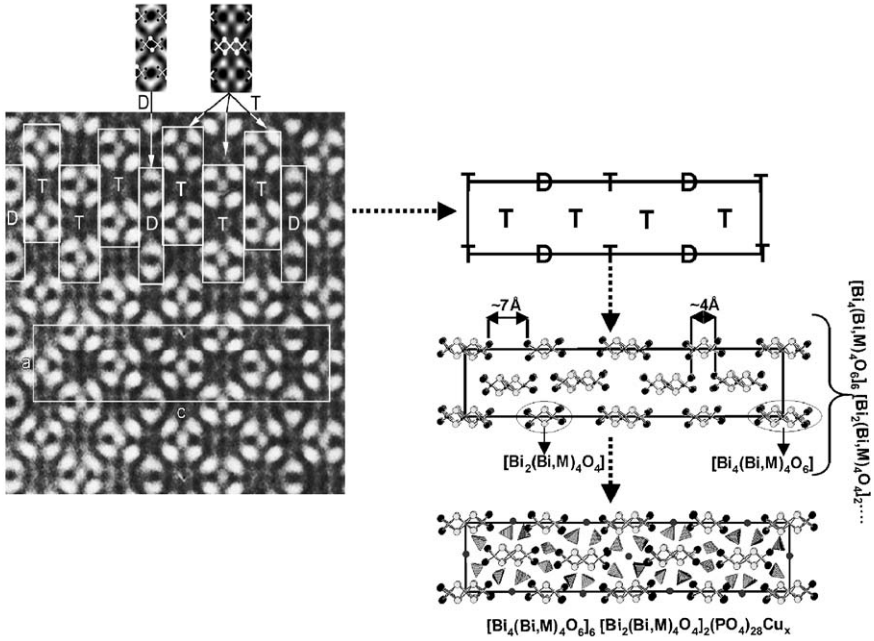

Fig. 3. Formulation of the new structure evidenced by ED and based on the [010] high-resolution image which highlighted the width and sequence of ribbons. From code already established (a_1) double ribbons are localized in dark region between two white circles (a)—(a_2) triple ribbons take place in dark region between two white crosses along (a). From experimental image (a_3), we deduced the new sequence: *tDtTtDt/TTtTTt*. Taking into account characteristics deduced from structures of compounds of the family (b,c), we obtained an average formula, starting point of the study and synthesis. (d) Image calculated on the basis of the atomic positions given by the X-ray results for a defocus of −10 nm and a thickness of 4.3 nm.

the single crystal dedicated section. It is also noteworthy that several prepared samples show an almost pure *DtTTt/TtDtT*-like phase ($c \sim 38$ Å) while attempts in other Bi_2O_3–P_2O_5–*M*O–CdO systems (*M* = Co, Zn, Ni) only yielded major *Tt/Tt*-like compounds ($c \sim 15$ Å). The most relevant results are presented in the Table 2. The indexed diagram of the pure powder is presented on Fig. 4.

Single crystals of the title compound have been prepared after heating at 930 °C and slow cooling until 830 °C (sweep = 2°C/h) of the powder corresponding to the $Bi_{18}Cd_{13}Cu_3(PO_4)_{14}O_{22}$ composition. Green needle-shaped single crystals have been isolated from the inhomogeneous melt. An energy dispersive spectroscopy analysis (GEOL JSM5300 microscope and PGT analysis system) performed on single crystals shows evidence of Bi, Cu, and Cd and P with a stoechiometry which roughly confirms the announced formula. Note that the majority of the tested crystals correspond to *DtTTt/TtDtT* crystal structure [18] as evidenced by their lattice parameters, $a = 11.544(5)$ Å, $b = 5.443(2)$ Å, $c = 38.574(21)$ Å. It points out the difficulties to synthesize crystals of this new phase since it decomposes in other related forms on melting.

5. Single crystal structural refinement

After absorption corrections from the crystal shape, the merging in different Laue group symmetries of the 12089 significant reflections ($I > 3\sigma(I)$) shows a strong preference for a monoclinic $2/m$ symmetry ($b = 5.416(4)$ as unique axis), $R_{int} = 8.81\%$ while other twofold axis choice in the 2/m symmetry as well as orthorhombic mmm symmetry yielded $R_{int} \sim 14\%$ despite the almost orthogonal unit cell. This small monoclinic distorsion has not been evidenced by ED study, which leads in a monoclinic cell to the extinction symbol A1-1 (means no glide plan) (Fig. 5). The *A* bravais lattice-only extinctions suggests possible *A*2, *Am* and *A*2/*m* space groups. No significant crystal structure difference was observed in the three space groups, so the centrosymmetric *A*2/*m* space group has been preferred. The crystal structure has been solved by the direct method calculation using SIR 97 [25] and has been refined with the JANA 2000 software [26] using a least-squares matrix on *F* an a unit weighting scheme. The 15 metal positions that form ribbons (labeled 1–15) have been located and assigned to Bi, Cd or Cu according to their weight. Additional atoms were deduced from the subsequent difference Fourier syntheses maps. The oxygen of the ribbons (O1–O6) are first found while seven phosphorus atoms and the tunnel cations (Cua, Cub, Cuc, Cud, Cue) have been located afterwards. At this stage, the introduction of the $hkl/\bar{h}kl$ twin favored by the β value $\sim 90°$, sensitively improved the refinement, i.e. ~5% loss in R_1, leading to $R_1 = 10.2\%$. Then, a mixed occupancy has been considered for the M8, M10 and M11, i.e. Bi/Cd8, Cd/Cu10 and Cd/Cu11 leading to a decrease of their thermal parameters. It is noteworthy that in the M10

Table 2
Different compositions tested to obtain the new phase observed by electronic microscopy with copper or with other metal transition cations

Composition	Major phase obtained	
M = Cu, Cd		
$Bi_{18}Cd_{12}Cu_4(PO_4)_{14}O_{22}$	*TtDtTtDt/TTtTTt* (monocl.)	$a = 11.4998(70)$ Å, $b = 5.4227(26)$ Å, $c = 53.5205(336)$ Å, $\beta = 90.09(5)^\circ$
$Bi_{18}Cd_{13}Cu_3(PO_4)_{14}O_{22}$	*TtDtTtDt/TTtTTt* (monocl.)	$a = 11.5039(56)$ Å, $b = 5.4285(22)$ Å, $c = 53.9203(229)$ Å, $\beta = 90.05(4)^\circ$
$Bi_{18}Cd_{10}Cu_6(PO_4)_{14}O_{22}$	*TtDtTtDt/TTtTTt* (monocl.)	$a = 11.4853(40)$ Å, $b = 5.4241(15)$ Å, $c = 53.5691(149)$ Å, $\beta = 90.03(3)^\circ$
$Bi_{18}Cd_{11}Cu_5(PO_4)_{14}O_{22}$	*DtTTt/TtDtT* (orthorh.) weak impurity lines	$a = 11.6563(47)$ Å, $b = 5.2782(15)$ Å, $c = 37.8131(135)$ Å
$Bi_{18}Cd_7Cu9(PO_4)_{14}O_{22}$	*DtTTt/TtDtT* (orthorh.) weak impurity lines	$a = 11.6614(48)$ Å, $b = 5.3247(16)$ Å, $c = 37.9634(128)$ Å
$Bi_{20}Cd_3Cu_{10}(PO_4)_{14}O_{22}$	*DtTTt/TtDtT* (orthorh.) weak impurity lines	$a = 11.5935(84)$ Å, $b = 5.2224(36)$ Å, $c = 37.6690(308)$ Å
$Bi_{24}Cd_2Cu_5(PO_4)_{14}O_{22}$	*DtTTt/TtDtT* (orthorh.) weak impurity lines	$a = 11.5987(66)$ Å, $b = 5.2192(20)$ Å, $c = 37.5513(211)$ Å
M = Ni, Cd		
$Bi_{18}Cd_{12}Ni_4(PO_4)_{14}O_{22}$	*Tt/Tt* (orthorh.)	$a = 11.3258(33)$Å, $b = 5.4884(16)$Å, $c = 15.2729(37)$Å
M = Zn, Cd		
$Bi_{18}Cd_{12}Zn_4(PO_4)_{14}O_{22}$	*Tt/Tt* (orthorh.)	$a = 11.3854(24)$Å, $b = 5.4960(12)$Å, $c = 15.2678(28)$Å
M = Co, Cd		
$Bi_{18}Cd_{12}Co_4(PO_4)_{14}O_{22}$	*Tt/Tt* (orthorh.)	$a = 11.3735(34)$Å, $b = 5.4946(15)$Å, $c = 15.2600(54)$Å

site, Cd^{2+} and Cu^{2+} have been split in adjacent positions in respect to the subsequent Fourier difference synthesis calculation. As already pointed out in [17–19] such mixed occupancy for edge-of-ribbons is responsible for the PO_4 multi configurations disorder around the central phosphorus atom. As a matter of fact, electron density peaks around P1-7 yielded one PO_4 (major) orientation around P2 and P5, two around P1, P3, P6, P7 while the most disordered P4 accepted three configurations. The strongly distorted PO_4 highlighted by P–O distances ranging from 1.44 to 1.9 Å and O–P–O angles from 87° to 138° are typical clues of a strong statistical disorder over several tetrahedra configurations. It is noteworthy that geometrical P–O and O–P–O restrictions have been used for some oxygen atoms. Considering the very stable occupancies for mixed positions Cd/Bi8 (0.43-0.57(4)), Cd/Cu10 (0.280–0.720(5)) and Cd/Cu11 (0.889/0.111(5)), the compound charge balance was controlled by fixing the total Cua + Cub + Cuc + Cud + Cue occupancy leading to $Occ._{Cua} = 0.88(7)$, $Occ._{Cub} = 0.40(6)$, $Occ._{Cuc} = 0.47(4)$, $Occ._{Cud} = 0.41(5)$, $Occ._{Cue} = 0.53(11)$. Hence the developed formula can be written $[O_6Bi_{4.57}Cd_{3.43}]_4^{+8.57}$ $[O_6Bi_4Cd_4]_2^{+8}$ $[O_4Bi_2Cd_{3.44}Cu_{0.56}]_2^{+6}$ $(PO_4)_{28}$ $Cu_{10.86}$. Because of residual electron density peaks around P and of possible deviation from the refined mixed positions occupancies, it is obvious that the refined crystal structure is ideal but does not perfectly reflect the occurring phenomena. At least the ordered ribbons framework and surrounding phosphorus and tunnels localization is correct. Atomic positions, isotropic equivalent displacement parameters for $Bi_{\sim 3.785}Cd_{\sim 3.575}Cu_{\sim 1.5}(PO_4)_{3.5}O_{5.5}$ are given in Table 3. Anisotropic displacement parameters are given in Table 4. High Resolution images were calculated on the basis of this atomic positions and match well with the experimental image for a defocus of –10 nm and a thickness of 4.3 nm (Fig. 3d).

6. Description

6.1. The ribbons framework

The pertinent bond distances are listed in Table 5. The Fig. 6 shows the projection along b of the ideal $Bi_{\sim 3.785}Cd_{\sim 3.575}Cu_{\sim 1.5}(PO_4)_{3.5}O_{5.5}$ crystal structure in which only one PO_4 configuration for P1-7 is shown in crown that represents the disordered area of the lattice. It ensues the validation of the proposed *TtDtTtDt/TTtTTt* model. For such disordered compounds, the ribbons based description enables to skip the Bi^{3+}/M^{2+} oxygen coordination, sometimes roughly defined, since disordered PO_4 are part of them. The independent ribbons are shown in Fig. 7. Triple $[O_6Bi_4Cd_4]_2^{+8}$ and double $[O_4Bi_2Cd_{3.44}Cu_{0.56}]_2^{+6}$ ribbons

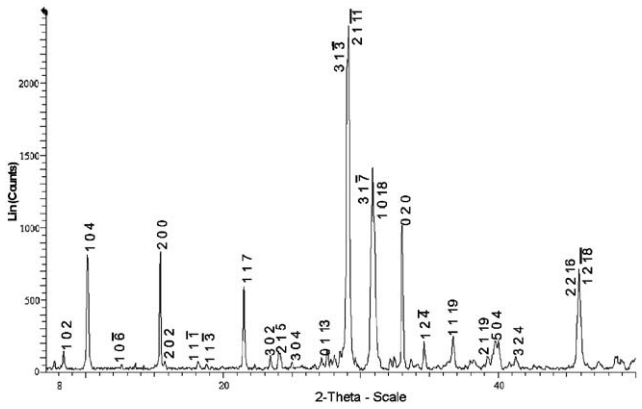

Fig. 4. Indexed XRD pattern for the monoclinic $Bi_{\sim 3.785}Cd_{\sim 3.575}Cu_{\sim 1.5}(PO_4)_{3.5}O_{5.5}$. The hkl indices confirm the A Bravais lattice because $k+l=2n$ for all reflections.

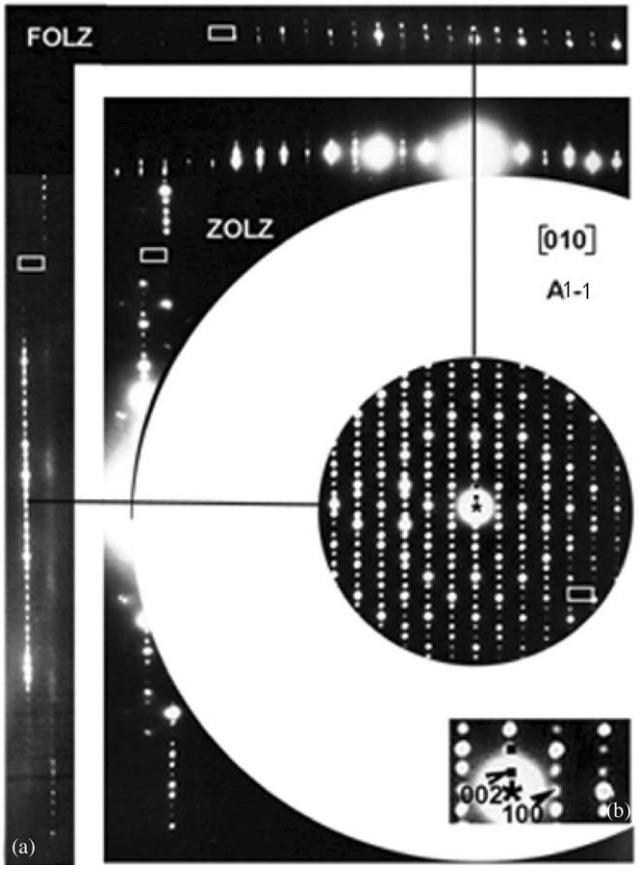

Fig. 5. [010] zone axis pattern realized. The comparison between the shift and difference of periodicity of the zero order Laue zone and first-order Laue zone leads to the partial symbol A1-1 of the monoclinic space group (-means no glide plan).

alternate along **c** at $x=0$ while only triple $[O_6Bi_{4.57}Cd_{3.43}]_4^{+8.57}$ alternates along c at $x=\frac{1}{2}$. As expected, the central cationic sites solely contain Bi^{3+} (e.g. Bi1-7) while Cd^{2+}, mixed Cu^{2+}/Cd^{2+} and Bi^{3+}/Cd^{2+} occupy edges of ribbons in respect to a strong preference for Cd^{2+}. The edge sharing $O(Bi,M)_4$ bricks show regular tetrahedral angles with typical O–M distances extending from 2.02 to 2.30 Å. The statistic distribution over PO_4 configurations picture the real mixed occupancy of edges of ribbons. One should recall that the perfectly ordered BiM_2XO_6 compounds (e.g. D/D like structure) only shows M^{2+} edges of ribbons.

It is true that despite the possibility of intergrowth defects due to the easy combination of ribbons along c, high-resolution photographs did not show these defects on the compounds studied so far. Therefore, we already described the $DtTTt/TtDtT$ as a regular intergrowth of the Tt/Tt and the D/D structure types [18]. In the same way, the new $TtDtTtDt/TTtTTt$ type shows many similarities with other compounds but none strict intergrowth between simpler sequences would lead to this structural type.

6.2. Monoclinic symmetry

Considering the refined crystal structure, one could wonder in what consists the monoclinic distortion while all of the compounds refined so far show an orthorhombic lattice. First, the possible systematic extinctions assorted with glide planes or helicoidal axes (other than included in the A Bravais lattice translations) existing in the previously adopted orthorhombic cells are largely violated. Fig. 8 shows the refined crystal structure with labels + and − that correspond to the height along b of the cations, in respect to the $O(Bi,M)_4$ tetrahedra formed structure. It is also noticeable that subsequent T ribbons along z are strongly shifted ($x\sim 0.48$ and 0.52). Then it follows that this shift combined with the ribbons structure avoids any two-fold axis and mirror symmetries except the $2/m$ along b.

6.3. Disorder

Several features depict the inter-ribbon zone disordered character. First, as shown in Fig. 9, the infrared spectra of the well-ordered $BiCu_2PO_6$ compound show a massif composed of a number of well-defined P–O bands between 750 and 1100 cm^{-1}. In this compound only one independent phosphorus position is found surrounded by one-only O_4 tetrahedron. By comparison are shown the IR spectra measured for the title compound and for $Bi_{\sim 1.2}Zn_{\sim 1.2}PO_{5.5}$ that both show a statistic distribution over several PO_4 configurations. For both disordered compounds, the observed spectra show wide massifs growing in the 750–1150 cm^{-1} zone. It is noteworthy that $Bi_{\sim 1.2}Zn_{\sim 1.2}PO_{5.5}$ ($a=11.214(1)$Å, $b=5.440(1)$Å, $c=14.809(2)$Å, SG *Icma*) only shows one central crystallographic phosphorus position

Table 3
Atomic positions and equivalent isotropic displacement parameters for $Bi_{\sim 3.785}Cd_{\sim 3.575}Cu_{\sim 1.5}(PO_4)_{3.5}O_{5.5}$

Atom	Wyck.	Occ.	x	y	z	U
Ribbons						
Bi1	4*i*		0.4184(3)	0.5	0.11167(8)	0.0262(9)
Bi2	4*i*		0.4206(4)	0	0.16243(7)	0.0257(11)
Bi3	4*i*		0.6342(3)	0	0.11151(8)	0.0254(9)
Bi4	4*i*		0.6336(3)	0.5	0.16313(7)	0.0242(10)
Bi5	4*i*		0.8969(4)	0	0.25044(9)	0.0294(11)
Bi6	4*i*		0.1135(4)	0	0.02386(7)	0.0289(12)
Bi7	4*i*		−0.1022(4)	−0.5	0.02677(7)	0.0292(11)
Cd/Bi8	4*i*	0.43/0.57(4)	0.4223(6)	0	0.06244(12)	0.035(2)
Cd9	4*i*		1.1105(6)	0	0.20349(12)	0.026(2)
Cd/Cu10	4*i*	0.280/0.719(5)	0.071(2)	0	0.3043(5)	0.026(4)
			0.1095(13)		0.2916(3)	
Cd/Cu11	4*i*	0.889/0.111(5)	0.6207(9)	0.5	0.0672(2)	0.050(3)
Cd12	4*i*		0.1151(6)	0.5	0.07160(12)	0.0220(16)
Cd13	4*i*		0.4264(5)	0.5	0.21134(11)	0.0214(16)
Cd14	4*i*		−0.0702(6)	0	0.07664(14)	0.034(2)
Cd15	4*i*		0.6059(6)	0	0.21438(10)	0.0243(17)
O1	8*j*		0.529(3)	0.256(9)	0.1368(7)	0.017(6)
O2	4*g*		0	−0.751(12)	0	0.022(12)
O3	8*j*		0.528(3)	0.249(9)	0.0878(6)	0.017(7)
O4	8*j*		0.007(3)	0.250(9)	0.2742(6)	0.021(7)
O5	8*j*		0.521(3)	0.251(8)	0.1856(6)	0.022(8)
O6	8*j*		0.015(3)	0.249(8)	0.0509(6)	0.024(8)
Tunnels						
Cua	2*c*	0.88(7)	0.5	0	0	0.026(4)
Cub	4*i*	0.40(6)	0.015(3)	0	0.1387(6)	0.018(13)
Cuc	8*j*	0.47(4)	1.0147(19)	0.148(5)	0.1391(4)	0.038(7)
Cud	4*h*	0.41(5)	0.5	−0.268(9)	0	0.049(14)
Cue	4*i*	0.53(11)	0.928(13)	0	0.368(3)	0.051(5)
PO_4						
P1	4*i*		0.712(2)	0	0.0420(5)	0.033(5)
Op11	4*i*		0.800(5)	0	0.0207(10)	0.042(10)
Op12	8*j*	0.5	0.710(9)	0.30(2)	0.0462(17)	0.042(10)
Op13	8*j*	0.5	0.757(8)	−0.16(2)	0.0630(17)	0.042(10)
Op14	8*j*	0.5	0.582(8)	0.134(19)	0.0376(17)	0.042(10)
P2	4*i*		0.341(2)	0	0.2471(5)	0.054(11)
Op21	4*i*		0.399(15)	0	0.271(3)	0.16(3)
Op22	8*j*		0.393(10)	0.27(2)	0.2249(18)	0.16(3)
Op23	4*i*		0.200(15)	0	0.244(3)	0.16(3)
P3	4*i*		0.208(2)	0	0.1030(6)	0.050(10)
Op31	4*i*		0.331(8)	0	0.1166(18)	0.109(12)
Op32	8*j*	0.5	0.198(4)	0.212(15)	0.0881(13)	0.109(12)
Op33	4*i*	0.5	0.146(10)	0	0.1332(19)	0.109(12)
Op34	4*i*	0.5	0.238(10)	0	0.075(2)	0.109(12)
Op35	8*j*	0.5	0.128(6)	0.212(15)	0.1032(13)	0.109(12)
P4	4*i*		0.333(3)	−0.5	0.0312(5)	0.039(6)
Op41	4*j*	0.5	0.199(18)	−0.5	0.028(3)	0.063(15)
Op42	8	0.5	0.381(11)	−0.75(2)	0.027(2)	0.063(15)
Op43	4*i*		0.318(7)	−0.5	0.0564(16)	0.063(15)
Op44	8*j*	0.25	0.416(16)	−0.38(4)	0.012(3)	0.063(15)
Op45	8*j*	0.25	0.33(2)	−0.77(5)	0.014(4)	0.063(15)
Op46	8*i*	0.25	0.20(2)	−0.35(5)	0.019(4)	0.063(15)
P5	4*i*		1.184(2)	−0.5	0.3198(5)	0.052(11)
Op51	4*i*		1.260(7)	−0.5	0.3409(14)	0.048(9)
Op52	4*i*		1.047(6)	−0.5	0.3265(14)	0.048(9)
Op53	8*j*		1.209(4)	−0.735(11)	0.3050(9)	0.048(9)
P6	4*i*		1.142(2)	0	0.3889(7)	0.095(19)
Op61	4*i*		1.269(10)	0	0.384(2)	0.10(3)
Op62	4*i*	0.5	1.01(2)	0	0.364(4)	0.10(3)
Op64	8*j*	0.5	1.114(7)	0.193(18)	0.410(2)	0.10(3)
Op65	4*i*	0.5	1.06(2)	0	0.412(3)	0.10(3)
Op66	8*j*	0.5	1.194(16)	0.30(4)	0.400(3)	0.10(3)

Table 3 (*continued*)

Atom	Wyck.	Occ.	*x*	*y*	*z*	*U*
P7	4*i*		0.212(3)	0.5	0.1761(5)	0.067(14)
Op71	4*i*		0.313(10)	0.5	0.153(2)	0.09(2)
Op72	8*j*	0.5	0.261(13)	0.23(3)	0.190(3)	0.09(2)
Op73	4*i*	0.5	0.89(2)	0	0.351(4)	0.09(2)
Op74	8*j*	0.5	0.148(14)	0.26(3)	0.166(3)	0.09(2)
Op75	4*i*	0.5	0.25(2)	0.5	0.203(4)	0.09(2)

Table 4
Anisotropic displacement parameters (in $Å^2$) for $Bi_{\sim 3.785}Cd_{\sim 3.575}Cu_{\sim 1.5}(PO_4)_{3.5}O_{5.5}$

Atom	U_{11}	U_{22}	U_{33}	U_{12}	U_{13}	U_{23}
Bi1	0.0195(13)	0.0216(16)	0.0375(18)	0	−0.0081(17)	0
Bi2	0.0189(18)	0.0264(19)	0.0316(18)	0	−0.0013(14)	0
Bi3	0.0163(12)	0.0256(17)	0.0343(16)	0	−0.0037(17)	0
Bi4	0.0242(17)	0.0207(18)	0.0275(16)	0	−0.0075(13)	0
Bi5	0.023(2)	0.0268(17)	0.0381(18)	0	−0.0139(15)	0
Bi6	0.0217(19)	0.026(2)	0.039(2)	0	0.0049(16)	0
Bi7	0.028(2)	0.0228(18)	0.037(2)	0	0.0150(15)	0
Cd8	0.027(3)	0.032(4)	0.047(4)	0	−0.014(3)	0
Cd9	0.018(3)	0.036(4)	0.026(3)	0	−0.007(3)	0
Cd10	0.015(6)	0.033(7)	0.032(8)	0	−0.012(5)	0
Cu10	0.015(6)	0.033(7)	0.032(8)	0	−0.012(5)	0
Cd11	0.044(5)	0.027(4)	0.080(6)	0	0.043(5)	0
Cd12	0.023(3)	0.009(3)	0.034(3)	0	−0.014(3)	0
Cd13	0.016(2)	0.020(3)	0.029(3)	0	0.007(2)	0
Cd14	0.020(3)	0.043(4)	0.040(4)	0	0.004(3)	0
Cd15	0.026(3)	0.025(3)	0.022(3)	0	0.001(2)	0
P2	0.015(11)	0.12(3)	0.026(12)	0	−0.005(8)	0
P3	0.014(9)	0.056(18)	0.08(2)	0	−0.021(11)	0
P5	0.024(11)	0.10(3)	0.028(11)	0	−0.012(9)	0
P6	0.034(12)	0.22(5)	0.031(13)	0	0.015(14)	0
P7	0.033(13)	0.14(4)	0.032(13)	0	0.009(10)	0

splitted in two independent P1 and P2 sites while the title compound ($a = 11.506(8)Å$, $b = 5.416(4)Å$, $c = 53.94(4)Å$, $\beta = 90.10(1)^\circ$, SG $A2/m$) shows seven independent P1-7 atoms. Hence, the comparable massif broadness for the two compounds mostly reflects the O_4 orientation disorder around a central P atom that yield to the overlapping and broadening of a number of bands.

Another viewing of the disorder is highlighted on neutron diffraction patterns versus XRD patterns. The large absorption cross section for Cd avoids neutron diffraction experiments on the synthesized $TtDtTtDt/TTtTTt$ compounds. Therefore, it appears rather interesting to qualitatively compare $BiCu_2PO_6$ (ordered D/D type) and disordered $Bi_{\sim 6.2}Cu_{\sim 6.2}P_5O_{28}$ (disordered $DtTTt/TtDtDtT$ type) that show comparable densities, e.g., 6.48 versus 6.70 g/cm^3. It clearly appears that XRD patterns measured in identical experimental conditions show approximately the same number of intense peaks and signal/background ratio due to their comparable Bi–M–O ribbons framework (Fig. 10a). Their neutrons diffraction patterns taken in the same conditions (m sample ~5 g, diffractometer D2b ILL-Grenoble-France, $\lambda = 1.593$ Å) drastically differ, since $BiCu_2PO_6$ shows a number of strong and well defined lines in the full 2θ-range, while $Bi_{\sim 6.2}Cu_{\sim 6.2}P_5O_{28}$ pattern only shows about twenty intense and medium lines in 0–90° range, then only weak lines appear at higher 2θ-range values (Fig. 10b). It is true that the c parameter differs between the two compounds, but note that the main ND pattern appearance is similar to all the disordered compounds that we investigated so far, independently of the unit cell size. Informative conclusions can be drawn out of this set of experiments:

(i) The background of both ND and XRD patterns show the same order of magnitude, involving no

Table 5
Selected bond lengths (Å) for $Bi_{\sim 3.785}Cd_{\sim 3.575}Cu_{\sim 1.5}(PO_4)_{3.5}O_{5.5}$

Oi–Bj	Dist (Å)	Oi–Bj	Dist (Å)
O1–Bi1	2.27(4)	O4–Bi5 (iii)	2.25(4)
O1–Bi2	2.32(4)	O4–Bi5 (iv)	2.19(4)
O1–Bi3	2.29(4)	O4–Cd9 (iv)	2.26(4)
O1–Bi4	2.28(4)	O4–Cd/Cu10	2.23(4)/2.02(5)
O2–Bi6 (vii)	2.27(4)	O5–Cd13	2.22(4)
O2–Bi6 (viii)	2.27(4)	O5–Bi2	2.18(4)
O2–Bi7	2.30(4)	O5–Bi4	2.23(4)
O2–Bi7 (viii)	2.30(4)	O5–Cd15	2.28(4)
O3–Bi3	2.22(4)	O6–Bi6	2.28(4)
O3–Bi1	2.25(4)	O6–Bi7 (viii)	2.31(4)
O3–Cd/Cu8	2.27(4)	O6–Cd14	2.17(4)
O3–Cd/Cu11	2.05(4)	O6–Cd12	2.10(4)

Pi–Oj	Distance (Å)	Oh–Pi–Oj	Angle (°)	Pi–Oj	Distance (Å)	Oh–Pi–Oj	Angle (°)
P1–Op11	1.54(6)	Op11–P1–Op12	97(4)	P5–Op51	1.44(8)	Op51–P5–Op52	115(4)
P1–Op12	1.61(11)	Op11–P1–Op13	109(4)	P5–Op52	1.61(8)	Op51–P5–Op53	108(3)
P1–Op13	1.53(10)	Op11–P1–Op14	119(4)	P5–Op53 x2	1.53(6)	Op53–P5–Op53	101(1)
P1–Op14	1.67(10)	Op12–P1–Op13	118(5)			Op52–P5–Op53	107(3)
		Op12–P1–Op14	93(9)	P6–Op61	1.49(12)	Op61–P6–Op62	127(8)
		Op13–P1–Op14	117(5)	P6–Op62	1.9(2)	Op61–P6–Op64 x2	109(5)
P2–Op21	1.44(16)	Op21–P2–Op22 x2	113(5)	P6–Op64 x2	1.56(11)	OP64–P6–OP64	112(1)
P2–Op22 × 2	1.97(11)	Op21–P2–Op23	117(9)			Op62–P6–Op64 x2	109(6)
P2–Op23	1.62(17)	Op22–P2–Op22	109(1)	P6–OP62	1.9(2)	Op62–P6–Op65	96(10)
		Op22–P2–Op23 x2	101(5)	P6–Op65	1.54(18)	Op62–P6–Op66 x2	118(6)
P3–Op31	1.59(10)	Op31–P3–Op32 x2	109(3)	P6–Op66 x2	1.81(19)	OP66–P6–OP66	120(1)
P3–Op32 × 2	1.40(8)	Op32–P3–Op33 x2	119(3)			Op65–P6–Op66 x2	87(7)
P3–Op33	1.78(11)	Op31–P3–Op33	89(8)	P7–Op71	1.72(12)	Op71–P7–Op72 x2	97(1)
		Op32–P3–Op32	105(1)	P7–Op72 x2	1.73(17)	Op71–P7–Op73	107(1)
P3–Op31	1.59(10)	Op31–P3–Op34	105(6)	P7–Op73	1.51(24)	Op72–P7–Op72	105(1)
P3–Op34	1.56(12)	Op31–P3–Op35 x2	124(3)			Op72–P7–Op73 x2	122(1)
P3–Op35	1.47(8)	Op34–P3–Op35 x2	98(4)	P7–Op71	1.72(12)	Op71–P7–Op74 x2	97(1)
		Op35–P3–Op35	88(2)	P7–Op74 x2	1.59(17)	Op71–P7–Op75	119(11)
P4–Op41	1.6(2)	Op41–P4–Op42 x2	108(1)	P7–Op75	1.5(2)	Op74–P7–Op74	111(1)
P4–Op42 × 2	1.48(13)	Op42–P4–Op42	120(1)			Op74–P7–Op75 x2	117(7)
P4–Op43	1.46(3)	Op41–P4–Op43	101(2)				
		Op42–P4–Op43	109(2)				
P4–Op43[a]	1.46(3)	Op43–P4–Op44	134(7)				
P4–Op44[a]	1.55(18)	Op43–P4–Op45	120(2)				
P4–Op45[a]	1.7(3)	Op43–P4–Op46	100(1)				
P4–Op46[a]	1.9(2)	Op44–P4–Op45	99(7)				
		Op44–P4–Op46	92(7)				
		Op45–P4–Op46	104(2)				

(i) $1/2+x, 3/2-y, z$, (ii) z, (iii) $-x, -y, 1-z$, (iv) $1/2-x, 1/2-y, 1-z$, (v) $1/2+x, -1/2-y, 1+z$,(vi) $1/2+x, 1/2-y, 1+z$, (vii) $-x, 1-y, -z$ (viii) $-x, -1-y, -z$.

[a]Two (OP43–OP44–OP45–OP46) tetrahedral configurations related by a mirror plane are statically distributed around P4.

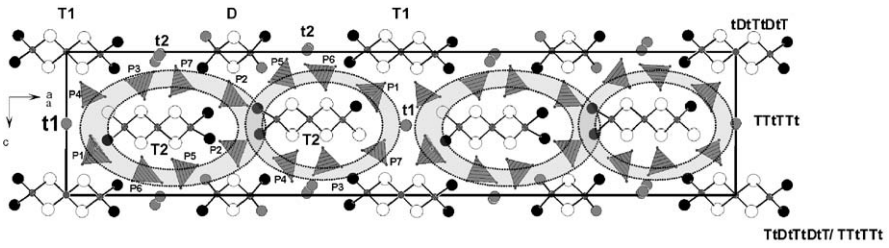

Fig. 6. Projection along the (010) direction of the $Bi_{\sim 3.785}Cd_{\sim 3.575}Cu_{\sim 1.5}(PO_4)_{3.5}O_{5.5}$ structure: the gray circles show the disorder zones.

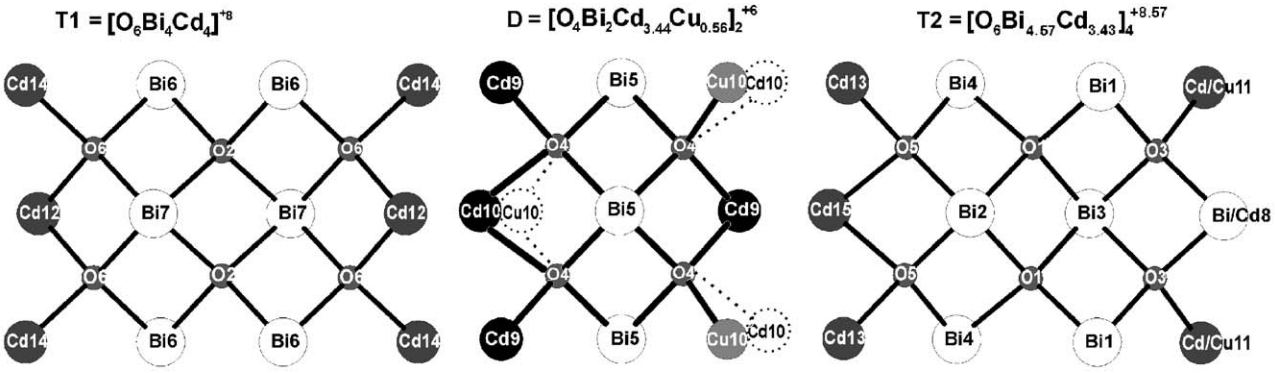

Fig. 7. Triple $[O_6Bi_4Cd_4]^{+8}$, $[O_6Bi_{4.57}Cd_{3.43}]^{+8.57}$ ($T=3$ tetrahedra wide) and double $[O_4Bi_2Cd_{3.44}Cu_{0.56}]^{+6}$ ($D=2$ tetrahedra wide) ribbons with the label scheme. Each oxygen is tetrahedrally coordinated by Bi, Cd and Cu.

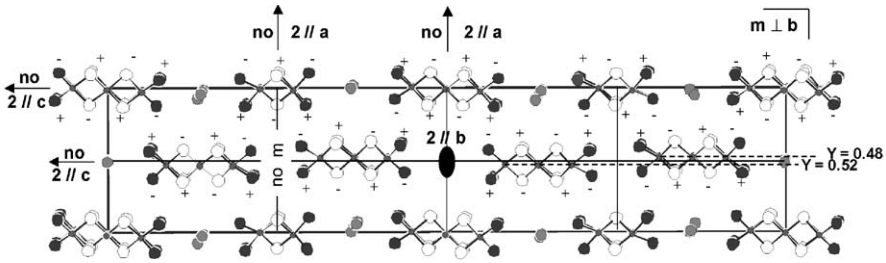

Fig. 8. View of the refined structure of $Bi_{\sim 3.785}Cd_{\sim 3.575}Cu_{\sim 1.5}(PO_4)_{3.5}O_{5.5}$ along the *b*-axis explaining the monoclinic symmetry to the existence or non-existence of symmetry elements +/− labels evidences the *y* coordinate sign of the polycationic ribbons.

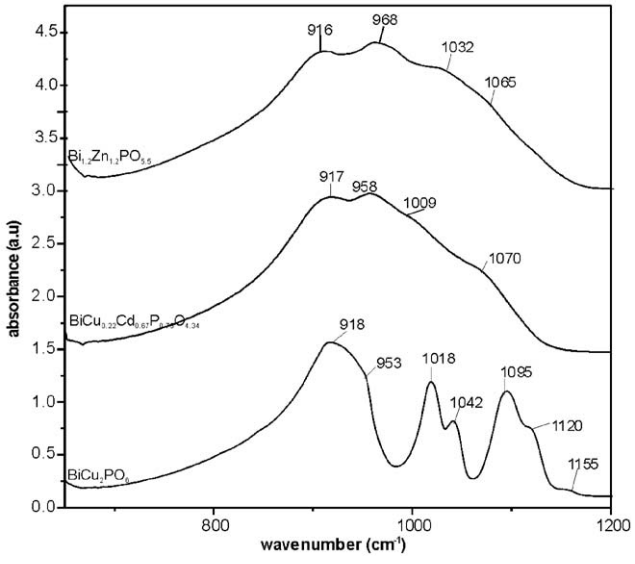

Fig. 9. Infrared spectrum for the $Bi_{\sim 3.785}Cd_{\sim 3.575}Cu_{\sim 1.5}(PO_4)_{3.5}O_{5.5}$ compound showing similar shape that the spectrum of the disordered $Bi_{\sim 1.2}Zn_{\sim 1.2}PO_{5.5}$ compound, but different compared to that of the ordered $BiCu_2PO_6$ compound.

short range ordering phenomena. This supports the ED observations on disordered materials that rarely show diffuse streaks but often commensurate or not additional spots ($q^* = (2/3 - \varepsilon)b^*$ in this study).

(ii) The difference observed between the ND and XRD patterns shapes mainly involve the oxygen role for the "disorder" phenomena. The Bismuth versus PO_4 high contrast in XRD structure factors comfort the ordered/disorder interface delimited by ribbons.

(iii) The great number of weak lines appearing on the $Bi_{\sim 6.2}Cu_{\sim 6.2}P_5O_{28}$ ND pattern are relevant to two phenomena: First, it denotes the statistical distribution of PO_4 oxygen positions towards a number of surrounding positions. In other words, the PO_4 strong disorder leads to homogenize the atomic planes densities—comparably to an amorphization process—yielding a tendency towards a monotone structure factors distribution in the full 2θ-range. Second, as a matter of fact, such phenomena may be assorted with oxygen Debye Waller coefficients increasing, i.e., lowering of the high 2θ- range intensities but low temperature does not modify the main neutron diffraction patterns shape.

6.4. Tunnels occupancy

Cub, Cuc and Cue take place in tunnels ($=t_1$) running along $<0,\ y,\ \sim.14>$ and delimited by $P3O_4$, $P5O_4$, $P6O_4$, $P7O_4$ while Cua and Cud stand along $\langle \frac{1}{2}, y, 0\rangle$ in tunnels ($=t_2$) formed by $P1O_4$ and $P4O_4$. Then, t_1 lies between one *D* and one *T* ribbon while t_2 lies between

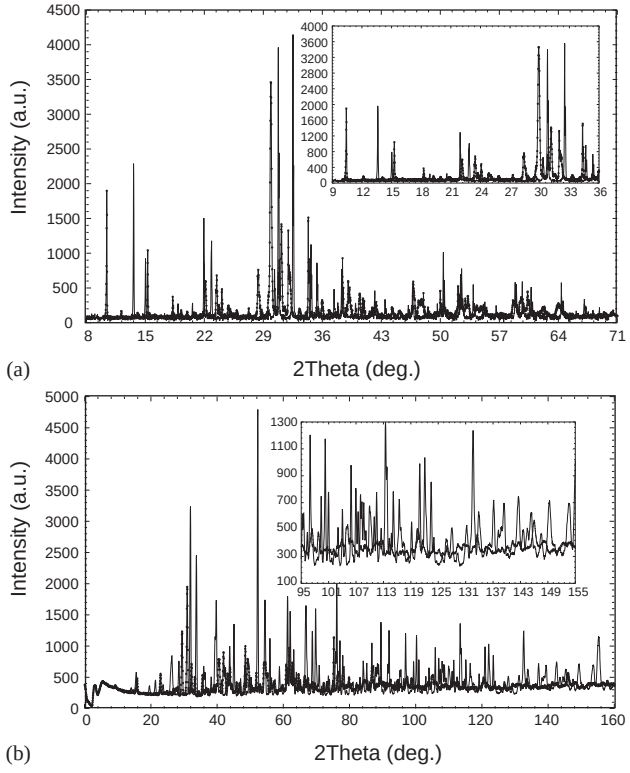

Fig. 10. Superposition of ordered ($BiCu_2PO_6$) and disordered ($Bi_{\sim 6.2}Cu_{\sim 6.2}P_5O_{28}$) X-ray and neutron powder patterns recorded in identical experimental conditions: (a) comparable X-ray diagrams due to the Bi–M–O ribbons framework and (b) neutron diagrams highlighted a disorder due to oxygen splitting over several independent PO_4 groups.

two subsequent T ribbons. Despite the strong disorder observed over PO_4 configurations, it is sometimes possible to deduce the tunnels cations environment and sequence from crystallographic and chemical considerations. Possible intra-tunnel ordering has so been successfully established for $Bi_{\sim 6.2}Cu_{\sim 6.2}P_5O_{28}$ and $Bi_{\sim 3}Cd_{\sim 3.72}M_{\sim 1.28}P_3O_{17}$ (M = Co, Cu, Zn) from refined occupancies [18–19]. In the title compounds of formula $[O_6Bi_{4.57}Cd_{3.43}]_4^{+8.57}$ $[O_6Bi_4Cd_4]_2^{+8}$ $[O_4Bi_2Cd_{3.44}Cu_{0.56}]_2^{+6}$ $(PO_4)_{28}$ $Cu_{10.86}$, considering a minimal intra-tunnel Cu–Cu distance of $b/2 \sim 2.7$ Å, the maximal Cu^{2+} number per formula units should be 12/f.u. So the refined 10.86 value 10.86/12 = 90.5% of intra-tunnel compacity and an average Cu–Cu distances of 2.7 Å/0.905 = 2.98 Å. Fig. 11a shows the $t1$ section with all the Cu^{2+} tunnel guests and refined PO_4 configurations. Among the possible Cua/Cud ordering, the $(-Cud^{3.87}Cua^{3.87}Cud^{3.07}Cud)n$ sequence with the surrounding PO_4 configuration as shown in Fig. 11b would provide a possible arrangement, with respect to Cu–Cu separations of 3.87 and 3.07 Å and square pyramidal and octahedral Cu^{2+} environments with Cu–O included in the 1.88–2.41 Å range. Furthermore this sequence involves the participation of all the copper and oxygen atoms forming $t1$. In the same manner, in $t2$, two possible Cu^{2+} ordering can be deduced from the global scheme shown in Fig. 11c. The $(-Cud^{2.77}Cub-)n$ is shown in Fig. 11d and highlights square pyramids CuO_5 with 2.73 Å > Cu–O > 1.94 Å. The other possible $(-Cuc^{3.66}Cuc^{3.66}Cue^{3.66}Cud-)n$ involves square pyramids with 2.79 Å > Cu–O > 1.78 Å. In the crystal, the two latter segments may be statistically distributed over the t_2 sites. To go in further comments about this kind of possible ordering would be pure investigation without any superstructure refinement from single crystal XRD. As a matter of fact, the imprecision on the refined occupancies for such a number of neighboring positions does not allow to establish undoubtful tunnel ordering. Furthermore, the sequence proposed in t_1 involves a $2b$ periodicity and the two sequences competing in t_2 involve b and $2b$ periodicities, respectively. The ED patterns revealed the b-axis tripling for isotypic compounds but concerned a different chemical composition, i.e., crystals from the $BiCuCdPO_6$ preparation. At least can we conclude that it may appear rather difficult to get the expected average 2.98 Å Cu–Cu distance from the three deduced sequence, which come out from occupancies misevaluation in the crystal structure refinement.

7. Magnetic properties

The magnetic susceptibility of the polycrystalline $Bi_{36}Cd_{24}Cu_8$ O_{44} $(PO_4)_{28}O_{44}$ sample is presented in Fig. 12. By analogy with the general formula established from the HREM images $[Bi_2(Bi,M)_4O_4]_2$ $[Bi_4(Bi,M)_4O_6]_6$ $(PO_4)_{28}$ M_x, the relative Cu/Cd occupancy of edges of ribbons and tunnels is not known, but the crystal structure established for $[O_6Bi_{4.57}Cd_{3.43}]_4^{+8.57}$ $[O_6Bi_4Cd_4]_2^{+8}$ $[O_4Bi_2Cd_{3.44}Cu_{0.56}]_2^{+6}$ $(PO_4)_{28}$ $Cu_{10.86}$ indicates a strong Cd^{2+} preference for edges of ribbons and a strong preference of Cu^{2+} for tunnels. From room temperature to 50 K, the experimental data can be fitted with a Curie–Weiss law, $\chi = C/(T-\theta)$, with a Weiss temperature $\theta = -49\,K$, $p_{\mathrm{eff}} = 1.91\,\mu B/Cu^{2+}$. The negative value of θ is characteristic of antiferromagnetic interactions between the Cu^{2+} cations while p_{eff} is in accordance with the usual value for Cu^{2+} ($p_{\mathrm{eff}} = 1.8-1.9\,\mu B$). It is noteworthy that the susceptibility slightly deviates from the Curie–Weiss law under 50 K, probably imaging antiferromagnetic couplings due to tunnels occupancy by Cu^{2+}. Antiferromagnetic interactions between Cu^{2+} in edges of ribbons cannot be totally excluded but are not likely from both the sample stoechiometry and the cadmium preference in these positions. Furthermore, intra-tunnel Cu–Cu separations are averaged to ~2.9 Å within linear chains while edges of ribbons are distant from each other within 3.5 Å long bonds within zigzag connections.

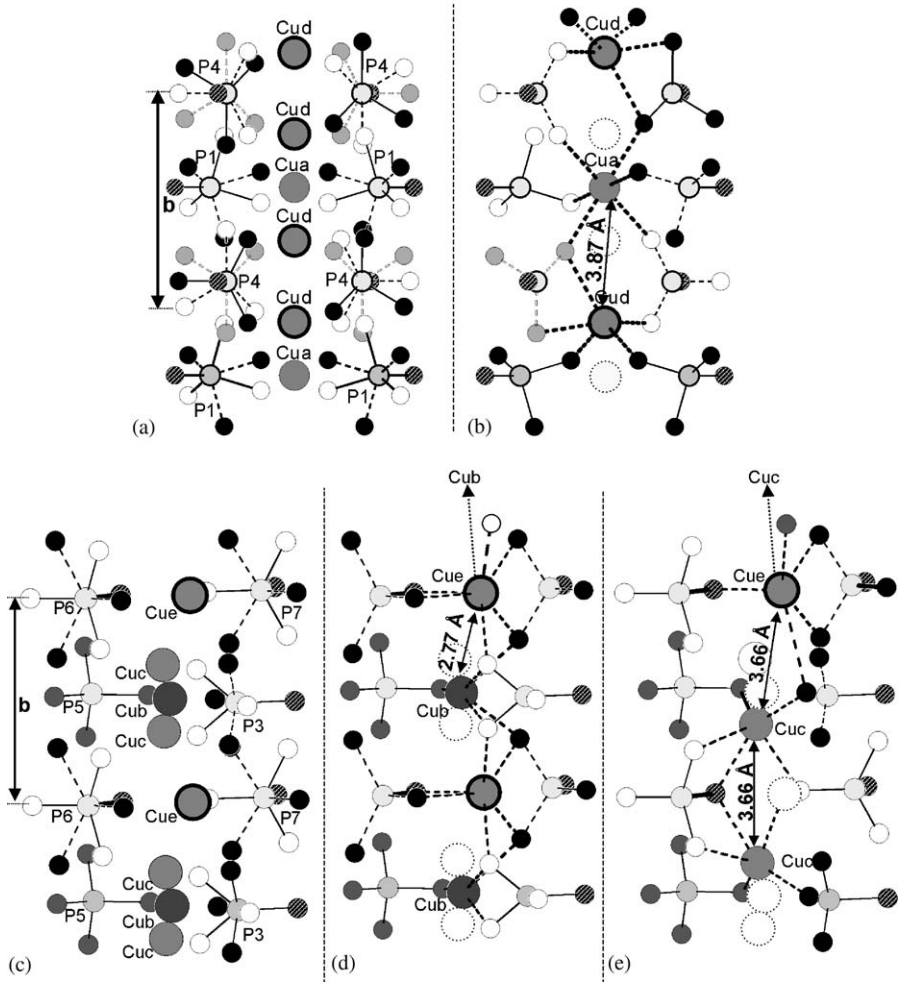

Fig. 11. (a) All surrounding PO_4 groups and Cu^{2+} guests in t_1 tunnels; (b) possible arrangement in t_1; (c) all surrounding PO_4 groups and Cu^{2+} guests in t_2 tunnels; (d) possible $(Cu_c–Cu_b)_n$ ordering in t_2; (e) possible $(Cu_c–Cu_c–Cu_e–Cu_b)_n$ sequence in t_2.

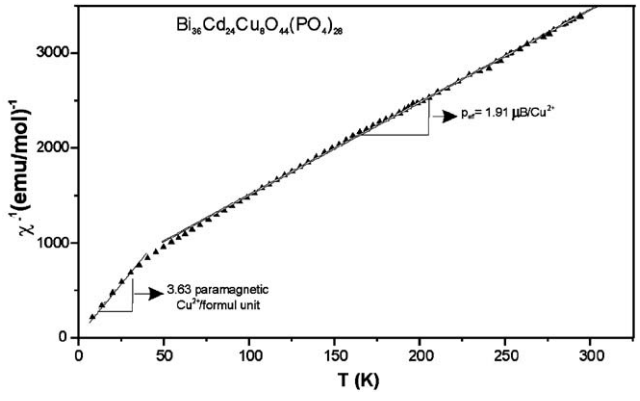

Fig. 12. Magnetic susceptibility for $Bi_{\sim 3.785}Cd_{\sim 3.291}Cu_{\sim 1.785}(PO_4)_{3.5}O_{5.5}$ compound.

Therefore the Curie law deduced from low temperature data is very approximate but leads to a paramagnetic contribution of 3.63 Cu^{2+} per formula unit (considering $p_{\text{eff}} = 1.91\,\mu B/Cu^{2+}$). These ~45% of paramagnetic Cu^{2+} are either located in edges of ribbons and would be isolated from each other by diamagnetic Cd^{2+} and Bi^{3+}. This would involve a partial Cd^{2+} occupancy in tunnels. The other possibility is that they stand in tunnels far from other Cu^{2+} yielding paramagnetism only.

References

[1] F. Abraham, M. Ketatni, Eur. J. Solid State Inorg. Chem. 32 (1995) 429.
[2] M. Ketatni, F. Abraham, O. Mentre, Solid State Sci. 1 (1999) 449.
[3] S. Nadir, J.S. Swinnea, H. Steinfink, J. Solid State Chem. 148 (1999) 295.
[4] X. Xun, S. Uma, A.W. Sleight, J. Alloys Compds. 338 (2002) 51.
[5] J. Huang, Q. Gu, A.W. Sleight, J. Solid State Chem. 105 (1993) 599.
[6] F. Abraham, M. Ketatni, G. Mairesse, B. Mernari, Eur. J. Solid State Chem. 31 (1994) 313.
[7] N. Tancret, Ph.D. Dissertation, Université des Sciences et des Technologies de Lille, France, Septembre 1995.
[8] A. Mizrahi, J.P. Wignacourt, H. Steinfink, J. Solid State Chem. 133 (1997) 516.

[9] M. Ketatni, B. Mernari, F. Abraham, O. Mentre, J. Solid State Chem. 153 (2000) 48.
[10] S. Giraud, A. Mizrahi, M. Drache, P. Conflant, J.P. Wignacourt, H. Steinfink, Solid State Sci. 3 (2001) 593.
[11] F. Abraham, M. Ketatni, B. Mernari, Adv. Mater. Res. 1 (1994) 2.
[12] X. Xun, S. Uma, A.W. Sleight, J. Solid State Chem. 167 (2002) 241.
[13] M. Ketatni, O. Mentré, F. Abraham, F. Kzaiber, B. Mernari, J. Solid State Chem. 139 (1998) 274.
[14] Digamber G. Porob, T.N. Guru Row, Acta Crystallogr. B 59 (2003) 606.
[15] O. Cousin, M. Huvé, P. Roussel, O. Perez, H. Steinfink, J. Solid State Chem. 165 (2002) 324.
[16] O. Cousin, O. Mentre, M. Huvé, F. Abraham, J. Solid State Chem. 157 (2001) 168.
[17] F. Abraham, O. Cousin, O. Mentre, El M. Ketatni,, J. Solid State Chem. 167 (2002) 168.
[18] M. Ketatni, M. Huve, F. Abraham, O. Mentre, J. Solid State Chem. 172 (2003) 327.
[19] M. Colmont, M. Huvé, M. Ketatni, F. Abraham, O. Mentré, J. Solid State Chem. 176 (2003) 221.
[20] M. Huvé, M. Colmont, O. Mentré. J. Mater. Chem. 16 (2004) 2628.
[21] JEMS software, P. Stadelmann, CIME-EPFL CH-1015, Lausanne, Switzerland, 2003.
[22] SAINT Plus version 5.00, Bruker Analytical X-ray Systems, Madison, WI, 1998.
[23] G.M. Sheldrick, SHELXTL NT, Program Suite for solution and Refinement of Crystal Structure, version 5.1, Bruker Analytical X-ray Systems, Madison, WI, 1998.
[24] SADABS: Program for absorption correction using SMART CCD based on the method of Blessing: Blessing, R. H., Acta Crystallogr. A 51 (1995) 33.
[25] A. Altomare, M.C. Burla, M. Camalli, G.L. Cascarano, C. Giacovazzo, A. Guagliardi, A. Grazia Giuseppina, G. Polidori, R. Spagna, J Appl. Crystallogr. 32 (1999) 115–119.
[26] V. Petricek, M. Dusek, JANA 2000. Institute of Physics, Praha, Czech Republic, 1997.